



Published in final edited form as:

Cancer Discov. 2020 September ; 10(9): 1374–1387. doi:10.1158/2159-8290.CD-19-1352.

## Chromatin Regulator, CHD1, Remodels the Immunosuppressive Tumor Microenvironment in PTEN-Deficient Prostate Cancer

Di Zhao<sup>1,2,#</sup>, Li Cai<sup>1,#</sup>, Xin Lu<sup>1,7,#</sup>, Xin Liang<sup>1,4</sup>, Jiexi Li<sup>1</sup>, Peiwen Chen<sup>1</sup>, Michael Ittmann<sup>6</sup>, Xiaoying Shang<sup>1</sup>, Shan Jiang<sup>3</sup>, Haoyan Li<sup>2</sup>, Chenling Meng<sup>2</sup>, Ivonne Flores<sup>3</sup>, Jian H. Song<sup>4</sup>, James W Horner<sup>3</sup>, Zhengdao Lan<sup>1</sup>, Chang-Jiun Wu<sup>3</sup>, Jun Li<sup>3</sup>, Qing Chang<sup>5</sup>, Ko-Chien Chen<sup>1</sup>, Guocan Wang<sup>1,4</sup>, Pingna Deng<sup>1</sup>, Denise J. Spring<sup>1</sup>, Y. Alan Wang<sup>1,\*</sup>, Ronald A. DePinho<sup>1,\*</sup>

<sup>1</sup>Department of Cancer Biology, The University of Texas MD Anderson Cancer Center, Houston, TX 77030, USA

<sup>2</sup>Department of Experimental Radiation Oncology, The University of Texas MD Anderson Cancer Center, Houston, TX 77030, USA

<sup>3</sup>Department of Genomic Medicine, The University of Texas MD Anderson Cancer Center, Houston, TX 77030, USA

<sup>4</sup>Department of Genitourinary Medical Oncology, The University of Texas MD Anderson Cancer Center, Houston, TX 77030, USA

<sup>5</sup>Institute for Applied Cancer Science, The University of Texas MD Anderson Cancer Center, Houston, TX 77030, USA

<sup>6</sup>Department of Pathology, Baylor College of Medicine, Houston, TX 77030, USA

<sup>7</sup>Department of Biological Sciences, University of Notre Dame, Notre Dame, IN 46556, USA

### Abstract

Genetic inactivation of *PTEN* is common in prostate cancer and correlates with poorer prognosis. We previously identified chromodomain-helicase-DNA-binding protein 1 (CHD1) as an essential gene in PTEN-deficient cancer cells. Here, we sought definitive *in vivo* genetic evidence for, and mechanistic understanding of, the essential role of CHD1 in PTEN-deficient prostate cancer. In *Pten* and *Pten/Smad4* genetically engineered mouse models, prostate specific deletion of *Chd1* resulted in markedly delayed tumor progression and prolonged survival. *Chd1* deletion was associated with profound tumor microenvironment remodeling characterized by reduced MDSCs and increased CD8+ T cells. Further analysis identified IL-6 as a key transcriptional target of CHD1, which plays a major role in recruitment of immunosuppressive MDSCs. Given the prominent role of MDSCs in suppressing responsiveness to immune checkpoint inhibitors (ICI),

\*Correspondence: Ronald A. DePinho (rdepinho@mdanderson.org; address: 1881 East Road, 3SCR5.4410, Houston, TX, 77054; Tel: 832-751-9756) or Y. Alan Wang (yalanwang@mdanderson.org; address: 1881 East Road, 3SCR5.4410, Houston, TX, 77054; Tel: 713-792-7928).

#These authors contributed equally to this work

**Conflict of interest:** R.A.D. is a founder, advisor and/or director of Tvardi Therapeutics, Inc., Nirogy Therapeutics, Inc., and Asyilia Therapeutics, Inc. which are focused on cancer, fibrosis and/or inflammation. The work of these entities is not related to the science of this manuscript. No potential conflicts of interest were disclosed by the other authors.

our genetic and tumor biological findings support combined testing of anti-IL-6 and ICI therapies, specifically in PTEN-deficient prostate cancer.

---

## INTRODUCTION

In human prostate cancer, genetic inactivation of *PTEN* occurs in 40% of cases and correlates with higher Gleason score, poorer prognosis, and increased metastasis (1,2). In the mouse, prostate-specific *Pten* deletion (*Pten<sup>PC-/-</sup>*) results in prostatic intraepithelial neoplasia (PIN) which slowly progresses to adenocarcinoma (3), indicating a gatekeeper function for PTEN in prostate cancer initiation. Additional evidence in humans also points to a role for PTEN in more advanced disease. Specifically, prostate cancer invariably becomes refractory to androgen deprivation therapy, resulting in the development of metastatic castration resistant prostate cancer with high morbidity and mortality. Notably, *PTEN* deletion or mutations are also enriched in this lethal subtype of prostate cancer (4,5), partially due to the cross-regulation between PTEN-AKT and androgen receptor (AR) signaling pathways (6–8). Finally, dual inactivation of PTEN and p53 or SMAD4 promotes locally invasive disease (9) or metastasis (10,11), respectively. In humans, PTEN and SMAD4 are key components of a prognostic signature predictive of lethality (10). Together, the central role of PTEN in prostate cancer has motivated efforts to identify therapeutic vulnerabilities in PTEN-deficient prostate cancer.

Chromodomain Helicase DNA Binding Protein 1 (CHD1) functions as a chromatin-remodeling factor, which alters nucleosome positioning and facilitates DNA transcription and replication (12). Loss of the *CHD1* gene occurs in ~7% of prostate cancer (TCGA data) and is considered a tumor suppressor gene in prostate cancer (13). More recently, loss of CHD1 in prostate cancer was found to contribute to DNA repair defects (14,15), as well as, transcriptional reprogramming by altering AR binding at lineage-specific enhancers (16). While CHD1 can be deleted in some human prostate cancers, it is rarely deleted in cases harboring PTEN inactivation or equivalent PI3K pathway alterations (17). Employing the concept of synthetic essentiality (18), we identified CHD1 as an essential effector of PTEN-deficient prostate and breast cancer cells (17). Accordingly, in prostate cancer cell lines or xenograft models, dual inactivation of PTEN and CHD1 resulted in growth arrest and impaired tumorigenesis (17,19). Mechanistically, PTEN loss inhibits ubiquitin-mediated degradation of CHD1, resulting in increased CHD1 levels that bind to histone 3 lysine 4 trimethylation (H3K4me3) mark and thereby activate NF- $\kappa$ B target genes involved in proliferation, apoptosis, and inflammation (17). Thus, CHD1 links PTEN to NF- $\kappa$ B, which has been shown to promote prostate cancer progression and alter the tumor microenvironment (TME) (20). At the same time, the critical downstream targets of CHD1 and the tumor biological mechanisms through which CHD1 promotes and maintains PTEN-deficient tumorigenesis are not known.

Targeting immune suppression mechanisms in the TME has revolutionized cancer treatment. While immune checkpoint inhibition (ICI) has yielded meaningful responses across many cancer types, clinical trials with anti-CTLA4 or anti-PD1 have shown minimal activity in prostate cancer patients (21–24). The poor response may relate to the impaired tumor-

specific antigen presentation (25) and/or presence of suppressive immunocytes such as myeloid-derived suppressor cells (MDSCs), regulatory T cells (Treg), and M2-type macrophages (26). In prostate cancer, MDSCs are a particularly abundant population that is known to suppress immune responses via a number of mechanisms, including inhibition of T cell proliferation and activation (27,28). In human prostate cancers, MDSCs have been identified as LIN<sup>-</sup> HLA-DR<sup>low/-</sup> CD11b<sup>+</sup> CD33<sup>+</sup> cells (28), and their abundance in the blood correlates with disease burden as reflected by circulating PSA levels in prostate cancer patients (29,30). In prostate cancer mouse models, MDSCs are identified as CD11b<sup>+</sup>Gr-1<sup>+</sup> cells, which can be further categorized into Gr-MDSCs (CD11b<sup>+</sup>Gr-1<sup>+</sup>Ly6G<sup>+</sup>) and Mono-MDSCs (CD11b<sup>+</sup>Gr-1<sup>+</sup>Ly6C<sup>+</sup>) (31,32). The critical role of MDSCs in prostate cancer has been validated by therapies targeting MDSCs or neutralizing MDSC recruiter cytokines in several prostate cancer mouse model studies (33,34). Notably, therapeutic inhibition of MDSCs has been shown to synergize with dual anti-PD1/CTLA4 therapy resulting in sustained control of disease in mouse models of metastatic CRPC (35).

Given the prominent role of *PTEN* loss and NF- $\kappa$ B activation in prostate cancer initiation and progression, respectively, we speculated that CHD1 and its downstream targets may serve to drive the initiation and progression of *PTEN*-null prostate cancer, possibly through modulation of the TME. In this study, we sought to secure rigorous genetic evidence of the synthetic essential role of CHD1 in the *Pten*-null prostate cancer model and determine the tumor biological mechanisms by which CHD1 serves as a critical effector of *Pten* deficiency in promoting prostate cancer progression. We show that deletion of *Chd1* in *Pten*-null models of prostate cancer profoundly impairs tumor progression in conjunction with dramatic remodeling of the TME towards an anti-tumor immune profile.

## RESULTS

### Genetic deletion of *Chd1* inhibits development of *PTEN*-null prostate cancer.

To understand more fully and definitively the role of CHD1 in *Pten*-deficient prostate cancer biology, a *Chd1* conditional knockout (*Chd1<sup>Loxp</sup>*) allele was crossed onto the prostate cancer model harboring *ARR2PB-Cre* (*PB-Cre*) or *Pten* conditional knockout allele (*Pten<sup>Loxp</sup>*) to generate *PB-Cre, Chd1<sup>L/L</sup>* and *PB-Cre, Pten<sup>L/L</sup>, Chd1<sup>L/L</sup>* genetically engineered mouse (GEM) models of prostate cancer (Fig. 1A). These models also contained a dual color fluorescent Cre-reporter allele, Rosa26-Loxp-tdTomato-Loxp-EGFP (Rosa-mTmG). In the absence of Cre recombinase, cells express tdTomato (mT) fluorescence; while Cre-expressing cells show EGFP fluorescence, which enables the tracking of GFP-positive cancer cells and early metastatic loci (Fig. 1A).

Prostate-specific deletion of *Chd1* (*Chd1<sup>Pc-/-</sup>*) resulted in no discernible histopathological changes in the prostate through ~20 months of observation (Supplementary Fig. S1A–B), consistent with a previous report (36). Prostate-specific deletion of *Pten* (*Pten<sup>Pc-/-</sup>*) produces high-grade prostatic intraepithelial neoplasia (PIN) and progresses slowly to adenocarcinoma (3). At 12 months of age, Magnetic Resonance Imaging (MRI) documented markedly delayed tumor development in *PtenChd1<sup>Pc-/-</sup>* mice relative to *Pten<sup>Pc-/-</sup>* controls (Fig. 1B–C), and histopathological analyses confirmed the less aggressive phenotype in the *Pten/Chd1<sup>Pc-/-</sup>* prostate tumors (Fig. 1D and Supplementary Fig. S1C).

Immunohistochemistry analysis further verified the efficient elimination of CHD1 as well as presence of *Pten*-loss induced AKT phosphorylation and activation (Fig. 1E). Phenotypically, *Chd1* deletion in the *Pten/Chd1<sup>pc-/-</sup>* prostate tumors resulted in significantly reduced tumor cell proliferation (Ki67 staining) (Fig. 1F and Supplementary Fig. S1D), elevated cancer cell apoptosis (Supplementary Fig. S1E), decreased CK8<sup>+</sup> luminal epithelial cells (Supplementary Fig. S1F), and significantly prolonged overall survival relative to *Pten<sup>pc-/-</sup>* controls (Fig. 1G). All *Pten/Chd1<sup>pc-/-</sup>* mice eventually succumbed to bladder outlet obstruction. Interestingly, in *Pten/Chd1<sup>pc-/-</sup>* mice older than 10-months of age, some focal lesions of adenocarcinoma expressed CHD1 protein (Supplementary Fig. S1G), consistent with incomplete Cre-mediated deletion of the conditional *Chd1* KO allele leading to rare outliers with tumor progression and earlier death in the *Pten/Chd1<sup>pc-/-</sup>* cohort.

To assess whether *Chd1* plays a similar critical role in prostate cancer models containing additional cancer promoting alleles, the impact of *Chd1* deletion was also examined in a highly aggressive metastatic prostate cancer model driven by prostate-specific co-deletion of *Smad4* and *Pten* (*Pten/Smad4<sup>pc-/-</sup>*) (10,33). MRI analyses showed that homozygous deletion of *Chd1* in this model led to marked reduced tumor volumes and weight at 4 months of age (Fig. 1H–I and Supplementary Fig. S1H). Histopathology analyses indicated that *Chd1* deletion caused delayed prostate cancer progression in the *Pten/Smad4<sup>pc-/-</sup>* mouse model (Supplementary Fig. S1I), along with reduced cell proliferation as well as increased cell apoptosis (Supplementary Fig. S1J). Using the *mTmG* reporter system, decreased GFP-positive micro-metastasis was documented in draining lumbar lymph nodes (Supplementary Fig. S1K–L). Specifically, 10 of 12 (83.3%) *Pten/Smad4<sup>pc-/-</sup>* mice (age >3 months) showed metastases versus 0 of 14 *Pten/Smad4/Chd1<sup>pc-/-</sup>* mice (Fig. 1J). Survival analysis indicated that deletion of *Chd1* prolonged the overall survival in the *Pten/Smad4<sup>pc-/-</sup>* mouse model to an even greater extent than the *Pten<sup>pc-/-</sup>* mouse model (Fig. 1K, and see discussion). Together, these data indicate that *Chd1* is dispensable in the normal prostate but plays an essential role in the development of *Pten*-null prostate cancers including metastatic disease.

### CHD1 promotes an immunosuppressive TME.

As a first step to understanding the tumor biological role of CHD1 in prostate cancer, we compared the RNA-seq transcriptional profiles of similarly sized *Pten<sup>pc-/-</sup>* and *Pten/Chd1<sup>pc-/-</sup>* prostate tumors collected from 4-month old mice. This unbiased analysis showed significant differences in inflammatory pathways including inflammatory response, IL-6-Stat3 signaling, and interferon response, among others (Fig. 2A and Supplementary Fig. S2A). The CHD1 inflammatory connection aligns with the capacity of CHD1 to regulate the NK- $\kappa$ B network (17), a major role in inflammation and tumorigenesis, prompting detailed cellular and molecular analysis of the *Pten<sup>pc-/-</sup>* and *Pten/Chd1<sup>pc-/-</sup>* prostate tumors.

Time of Flight Mass Cytometry (CyTOF) was used to provide high-dimensional analysis of immune cells and other TME components (37,38). CyTOF of *Pten<sup>pc-/-</sup>* (n=6) and *Pten/Chd1<sup>pc-/-</sup>* (n=5) tumors used a multi-marker panel for epithelium and tumor-infiltrating leukocytes, including T cell, B cell, NK cells, and myeloid cells. *Pten/Chd1<sup>pc-/-</sup>* tumors displayed less CD45<sup>+</sup> immune cells than in the *Pten<sup>pc-/-</sup>* tumors (Supplementary Fig. S2B). viSNE, a visualization tool for high-dimensional single-cell data based on the t-SNE

algorithm (39), revealed that the immunophenotype of *Pten*<sup>pc-/-</sup> tumors showed more abundant MDSCs and tumor-associated macrophages (TAMs), and fewer T cells, B cells and NK cells relative to *Pten/Chd1*<sup>pc-/-</sup> tumors (Fig. 2B–D). In addition, CHD1 status had a minimal impact on CD4<sup>+</sup> T cell, B cell and NK cell populations (Fig. 2C–D).

Comparative immunoprofiling was also performed in the aggressive metastatic *Pten/Smad4*<sup>pc-/-</sup> model to assess the impact of CHD1 on tumor biology and disease progression. Analysis of *Pten/Smad4/Chd1*<sup>pc-/-</sup> (n=5) versus *Pten/Smad4*<sup>pc-/-</sup> (n=6) tumors revealed that *Chd1* deletion is also associated with decreased MDSCs and increased CD8<sup>+</sup> T cells (Fig. 2E–F and Supplementary Fig. S2C), yet had no impact on TAMs, CD4<sup>+</sup> T cells and B cells (Supplementary Fig. S2D–E) and showed a considerable increase of NK cell infiltration (Supplementary Fig. S2C and S2F). Finally, we examined prostate tissues null or intact for *Chd1* alone, revealing no impact on immune cell populations (Supplementary Fig. S2G–I). Together, these results show that PTEN status contributes to the immune regulatory impact of CHD1, and that CHD1 regulates the abundance of immunosuppressive MDSCs and anti-tumor CD8<sup>+</sup> T cells in PTEN-deficient prostate cancer.

Immunoprofiling data were confirmed by the immunofluorescence staining of Ly6G and CD8<sup>+</sup> T cell markers (Fig. 3A–B). The MDSC gene signature analysis of TCGA database (33) showed that, in human prostate cancer, high CHD1 expression correlated with the enrichment of MDSCs (Fig. 3C and Supplementary Fig. S3A). The positive correlations between CHD1 expression and MDSC surface marker CD15 were also found in human prostate cancer samples (Fig. 3D). Meanwhile, IHC staining of CHD1 and CD8a in a human prostate cancer tissue microarray (N=72) showed that the tumors with high CHD1 expression were infiltrated with fewer CD8<sup>+</sup> T cells ( $r = -0.273$ ;  $p = 0.02$ ) (Fig. 3E–F). The negative correlation between CD8a and CHD1 expression was also observed in TCGA human prostate cancer database (Supplementary Fig. S3B).

### CHD1 controls MDSCs recruitment and IL-6 serves as a key mediator.

The crosstalk between cancer cells and tumor-infiltrating immunocytes is mediated by direct cell-cell interaction, such as PD-L1 and PD-1 binding, as well as by secreted factors such as cytokines and other stromal factors. To assess the potential presence of CHD1 regulated factors governing the recruitment of MDSCs in the prostate cancer TME, we performed migration and proliferation assays using serum-free conditioned medium derived from control versus *Chd1* knockdown murine *Pten*-deficient prostate cancer cell lines (Fig. 3G). Results showed that CHD1 depletion significantly suppressed the recruitment of MDSCs *in vitro* (Fig. 3H), yet had minimal impact on the activity of MDSCs (Supplementary Fig. S3C) or CD8<sup>+</sup> T cells (Fig. 3I and Supplementary Fig. S3D–E). These *in vitro* functional assays suggested that CHD1 may recruit MDSCs via a cytokine-dependent mechanism, and that the impact of CHD1 deficiency on T cell numbers may be due in part to the abundance of MDSCs, which are known to inhibit T cell proliferation and activation via NO production and secretion of Arg1 (27,28,33).

To gain insight into the molecular mediators of CHD1 in prostate cancer, we triangulated three datasets; specifically, (a) transcriptomes of tumors in the *Pten*<sup>pc-/-</sup> and *Pten/Chd1*<sup>pc-/-</sup> mouse models, (b) transcriptomes of isogenic human PTEN-null PC-3 cell lines wildtype or

null for *CHD1* (17), and (c) CHD1 ChIP-seq data of isogenic human PTEN-null PC-3 cell lines wildtype or null for *CHD1* (17). The integration of the cross-species tumor and cell line analyses identified 11 genes that were consistently regulated by CHD1 across the model systems and the species (Fig. 4A). To further narrow the candidate list, we then intersected CHD1 ChIP-seq on a murine *Pten*-deficient prostate cancer cell line, revealing only 4 direct CHD1 targets, including IL-6, PTX3, COL6A3 and PTHLH. Identification of the IL-6-Stat3 pathway in our analysis was significant given its known roles in inflammation and cancer progression (40,41); the capacity of IL-6 to stimulate MDSC activity in cancer (28,42,43); and the finding that IL-6R blockade eliminates MDSCs, enhances T-cell responses and suppresses tumor growth (44). Moreover, STAT3 inhibition in myeloid cells has been shown to reduce significantly intratumoral MDSCs and to increase CD4<sup>+</sup> and CD8<sup>+</sup> cells (34,45). A Gene Set Enrichment Analysis (GSEA) using Hallmark gene sets revealed that the IL-6-Stat3 pathway was up-regulated in *Pten*-loss prostate, whereas CHD1 depletion significantly suppressed IL-6-Stat3 signaling in this context (Fig. 4B), supporting a role for CHD1 in mediating PTEN regulation of the IL-6-JAK-STAT3 pathway in prostate cancer.

In furtherance of the CHD1-IL-6 link, ChIP-seq analysis revealed that CHD1 directly binds to the promoter region of the murine *IL-6* gene (Fig. 4C), which enabled identification of a novel CHD1-binding motif (TGAG/CTCA) (Fig. 4D). This motif is highly conserved in the human and mouse *IL-6* gene at positions -225 and -291, respectively, of the transcriptional start site (Fig. 4E). These data suggested that CHD1 directly binds to and regulates IL-6 gene expression. In addition, we found that the transcriptional regulation of the IL-6 gene by CHD1 was dependent on *PTEN*-loss (Supplementary Fig. S4A), and that CHD1 can cooperate with the NF- $\kappa$ B transcription factor in regulating IL-6 gene expression (Supplementary Fig. S4B). In light of CHD1's function in chromatin assembly, we also performed ATAC-seq in CHD1 wildtype vs. knockout LNCaP cells. Notably, CHD1 deletion reduced overall chromatin accessibility in gene promoter regions (Supplementary Fig. S4C), consistent with its classical function in opening chromatin in many genes. Upon CHD1 deletion, promoter accessibility of the *IL-6* gene were significantly decreased, indicating that CHD1 loss makes the *IL-6* locus less accessible (Supplementary Fig. S4D).

Meanwhile, human TCGA prostate cancer data analysis established that CHD1 expression levels correlates positively with IL-6 expression levels as well as with activated (phosphorylated) STAT3 protein levels (Fig. 4F-G and Supplementary Fig. S4E). Expression of IL-6 at both the mRNA and protein levels was significantly down-regulated in *Pten/Chd1<sup>PC</sup>-/-* vs. *Pten<sup>PC</sup>-/-* prostate tumors (Fig. 5A-B). Moreover, a ~1kb DNA fragment of human IL-6 promoter containing the CHD1 binding motif was inserted into a luciferase-expression construct, followed by introduction into control or CHD1 knockdown PC-3 cells. As shown in Fig. 5C and Supplementary Fig. S4F, the *IL-6* promoter could drive luciferase expression in the presence of CHD1, but not in the absence of CHD1, reinforcing that *IL-6* is a direct target gene of CHD1. Mutation of the CHD1-binding motif (TGAGTCA) in the *IL-6* promoter abolished luciferase reporter activity (Fig. 5D), consistent with an essential role of this putative CHD1-binding motif in mediating CHD1-directed transcriptional activation. Additionally, the capacity of CHD1 to regulate *IL-6* gene expression requires *PTEN* loss in prostate cancer (Supplementary Fig. S4G). Together, these results establish the Pten-Chd1-IL-6 pathway in prostate cancer.

To verify the CHD1-IL-6 axis in the control of MDSC recruitment, IL-6 secretion was measured in conditioned media derived from control and CHD1-depleted prostate cancer cells (Fig. 3G and Supplementary Fig. S4H). *In vitro* MDSC recruitment assays showed reduced MDSC migration with CHD1 depletion, which was partially rescued upon supplementation of the conditioned media with IL-6 recombinant protein (Fig. 5E). Moreover, anti-IL-6 or IL-6R antibody treatment of the conditioned media blocked MDSC migration (Fig. 5F), and this effect could be eliminated by CHD1 depletion (Supplementary Fig. S4I). Furthermore, immunofluorescence co-staining of IL-6R and the MDSC surface marker Ly6G in murine prostate tumor sections showed that tumor-infiltrating MDSCs were the major immune cell population associated with IL-6 protein secreted by prostate cancer cells (Supplementary Fig. S4J). Together, these data suggest that the PTEN-CHD1-IL-6 axis modulates the recruitment of immunosuppressive MDSCs into the prostate cancer tumor microenvironment.

### **Synergistic anti-tumor effect of CHD1/IL-6 inhibition in combination with ICI in prostate cancer.**

The poor response of prostate cancer to ICI in the clinic (23) and the key role of MDSCs in suppressing ICI responsiveness in mouse models (28,35,46,47), prompted us to test whether inhibition of the CHD1/IL-6 pathway would improve ICI responsiveness in various mouse models of prostate cancer. We first utilized a cell line (DX1) derived from a tumor arising in a metastatic chimeric prostate cancer mouse model containing GFP reporter, probasin-Cre transgene and conditional alleles of *Pten*, *Trp53*, and *Smad4* (CPPSML), where cancer-prone mice were generated by blastocyst injection of CPPSML-derived ES cells (35). A doxycycline (Dox) inducible *Chd1* knockdown element was introduced into DX1 cells, followed by orthotopic injection into the dorsolateral prostate of syngeneic C57BL/6J mice to produce cohorts with rapidly developing aggressive prostate cancer (Supplementary Fig. S5A). In this model, we tested the impact of CHD1 depletion on anti-PD1 responsiveness, revealing that combined CHD1 depletion and 5 treatments of anti-PD1 generated superior anti-tumor effect than either monotherapy in the CPPSML model (Fig. 6A–B).

Then, we evaluated the therapeutic effects of IL-6 inhibitor and/or anti-PD1/CTLA4 antibodies in spontaneous tumors arising in small cohorts of two models, CPPSML and *Pten/Smad4<sup>pc-/-</sup>* mice. In contrast to the slowly progressive *Pten<sup>pc-/-</sup>* model which rarely invades or metastasizes, these prostate models develop highly aggressive adenocarcinomas progressing rapidly with frequent metastasis and shorter overall survival. These more aggressive models were used in our therapeutic trials as they better recapitulate advanced disease in patients, providing a more relevant model for assessment of our therapeutic interventions. As shown in Fig. 6C–D, CPPSML mice exhibited *de novo* resistance to anti-PD1/CTLA4 treatment, as reported previously (35). Necropsy at one month following termination of treatment showed that 4 of 4 anti-IL-6-treated mice possessed sizeable tumors; whereas, 2 of 4 anti-IL6/PD1/CTLA4-treated mice showed elimination of disease and 2 of 4 exhibited minimal residual disease (Fig. 6C–D and Supplementary Fig. S5B–C). IL-6 blockade alone or in combination with ICI reduced MDSCs recruitment and increased CD8<sup>+</sup> T cell infiltration in the CPPSML tumors (Supplementary Fig. S5D). To reinforce the limited study, we also tested this treatment protocol in the *Pten/Smad4<sup>pc-/-</sup>* model, revealing

significant suppression of tumor growth in mice receiving combined anti-IL6 and anti-PD1/CTLA4 treatment (Fig. 6E–F and Supplementary Fig. S5E). Similarly, *Pten/Smad4<sup>pc-/-</sup>* tumor immune profiles showed reduced MDSC population and increased CD8<sup>+</sup> T cells in the combination treatment tumors (Fig. 6G and Supplementary Fig. S5F–G). Together, these preclinical data indicated that the combination of IL-6 inhibition and PD1/CTLA4 blockade provides more robust anti-tumor activity in various *Pten*-deficient mouse models of prostate cancer.

## DISCUSSION

In this study, we provide genetic evidence and tumor biological bases of the essential role of CHD1 in PTEN-deficient prostate cancers, where CHD1 plays an important tumor biological role in the recruitment of immunosuppressive MDSCs into the prostate cancer TME (Fig. 7). Integrated analysis identified IL-6 as a key downstream effector of CHD1, a finding consistent with previous insights that CHD1 activates the NF- $\kappa$ B network in PTEN-deficient prostate cancers and that IL-6 is a major target gene of NF- $\kappa$ B (17,48). The role of the PTEN/AKT/CHD1/IL-6 pathway in MDSC recruitment informed combination immune therapies with superior anti-tumor activity that provides a responder hypothesis for clinical trials in prostate cancer.

While our work identifies IL-6 as the key factor in MDSC recruitment, it is worth noting that we cannot exclude the possibility that other CHD1-regulated cytokines or chemokines also contribute to TME remodeling. For example, we also observed that CHD1 binds to the promoter of the COL6A3 gene (Fig. 4A), which encodes collagen type VI alpha 3 chains and which is known to induce the recruitment of macrophages and endothelial cells into the TME (49). Along these lines, reduced tumor associated macrophages in *Pten/Chd1<sup>pc-/-</sup>* prostate tumors, not in *Pten/Smad4/Chd1<sup>pc-/-</sup>*, underscores the need for future studies delineating the connections of CHD1, COL6A3 and M1/M2 macrophages, and to understand whether these connections are dependent on specific genotypes.

Previously, using the *Pten/Smad4<sup>pc-/-</sup>* prostate cancer mouse model, we reported that *Smad4* deficiency in the context of *Pten* loss led to a lethal prostate cancer phenotype with a high-rate of metastasis to lymph node and lung (10). We also demonstrated loss of SMAD4 results in a significant enrichment of MDSCs in prostate tumors by activating YAP and its downstream gene *CXCL5* (33), contributing to the aggressive phenotype observed in the *Pten/Smad4<sup>pc-/-</sup>* GEM model. When comparing the GEM models of *Pten/Chd1<sup>pc-/-</sup>* and *Pten/Smad4/Chd1<sup>pc-/-</sup>*, it is notable that CHD1 depletion in the *Pten/Smad4<sup>pc-/-</sup>* model led to a stronger inhibitory effect on MDSCs in prostate tumor. We propose that this phenomenon relates in part to increased MDSC infiltration and their prominent roles in the development of SMAD4-deficient prostate cancer. This SMAD4-MDSC connection may also explain why CHD1 inhibition shows a more significant anti-tumor impact in *Pten/Smad4*-null relative to *Pten*-null prostate cancer models.

Our previous human patient-derived xenograft and new GEM models of prostate cancer (this study) strongly validate CHD1 as a therapeutic target in PTEN-deficient prostate cancers. With respect to its therapeutic potential, it is also worth noting that CHD1-null prostates are



phenotypically normal (Supplementary Fig. S1A–B), belying an acceptable therapeutic window. Despite these encouraging factors, tumor progression was rarely observed in some *PtenChd1* KO mice although these cases appear to result from lack of Cre-mediated deletion of CHD1; nevertheless, continued study is warranted to identify potential second site suppression events that may underlie CHD1 bypass. In addition, recent work from others supports the view that CHD1 can act as a tumor suppressor gene, consistent with its recurrent deletions in the prostate cancer genome (50) or transcriptional reprogramming of AR signaling pathways (16). With respect to the former, we have observed that these CHD1 deletions occur in PTEN-intact cancers (17). With respect to the latter study, while CHD1 loss appeared to be permissive for tumor growth in a PTEN-deficient mouse model, it is difficult to draw such conclusions from this study based on the small animal cohort (n=5), low frequency of tumor progression (1 in 5 mice) and lack of survival data (16). In light of the fact that our ‘escapers’ showed lack of deletion of the conditional null allele, our work encourages further documentation of CHD1 expression in the outlier tumor to rule out incomplete CHD1 deletion as a cause for late (1 year old) tumor relapse or *bona fide* bypass mechanisms in *Pten/Chd1* deficient prostate cancer (16).

The majority of prostate cancer patients show primary or acquired resistance to immunotherapy, including dendritic cell–based cancer vaccine sipuleucel-T and single agent ICIs (22–24,51). Encouraging results from pre-clinical mouse model systems have highlighted the beneficial impact of co-targeting immune checkpoints and myeloid cells/their oncogenic signaling pathways (35,52,53). In this study, we expand the list of combinatorial therapies by highlighting the potential of inhibiting CHD1/IL-6 axis and immune checkpoint in *PTEN*-deficient prostate tumors. CHD1 inhibition using an inducible shRNA system showed synergistic tumor-suppressing effects when combined with anti-PD1 antibody in the syngeneic xenograft prostate cancer model. It suggests a potential application of CHD1 inhibitor, if developed in the future. Although several FDA approved inhibitors targeting the IL-6/JAK/STAT3 signaling pathway are being extensively investigated in preclinical studies and clinical trials (54), their activities against prostate cancer in clinical trials have not been encouraging (55,56). In the current study, preliminary preclinical experimental studies targeting IL-6 using antibodies in combination with anti-PD1/CTLA-4 arrested prostate progression in two prostate cancer models support the design of similar trials for patients with advanced prostate cancer, particularly those deficient for *PTEN*.

## METHODS

### Mouse Strains and breeding

*Pten<sup>Loxp</sup>*, *Smad4<sup>Loxp</sup>* and *Rosa-mTmG* mice have been described previously (10). *Chd1<sup>Loxp</sup>* allele were generated by breeding *Chd1tm1a(KOMP)Wtsi* strain mice with the FLP deleter strain B6.129S4-Gt(58)26Sortm1(FLP1)Dym/RainJ. Exon 16 of *Chd1* is flanked by two loxP sites. *Chd1<sup>Loxp</sup>* mice were crossed with PB-Cre mice to generate the prostate-specific *Chd1* knockout mouse model, and then bred with *Pten<sup>Loxp</sup>*, *Smad4<sup>Loxp</sup>* and *Rosa-mTmG* mice. Mice were interbred and maintained at UT MD Anderson Cancer Center, monitored for signs of ill-health every day, and euthanized and necropsied when moribund. All

manipulations were performed under the review and approval of MD Anderson Cancer Center's Institutional Animal Care and Use Committee.

### Immunohistochemistry and immunofluorescence

Immunohistochemistry was performed as previously described (17). A pressure cooker (95°C for 30 min followed by 120°C for 10 s) was used for antigen retrieval using Antigen Unmarking Solution (Vector Laboratories). Antibodies specific to CHD1 (Sigma, #HPA022236), AKT-473P (Cell Signaling, #4060s), Keratin 5 (BioLegend 905501), Cytokeratin-8 (BioLegend 904801), CD8 (Bioss bs-0648R), Ly6G (BioLegend 127601), CD15 (DAKO M3631), IL-6R (R&D Systems AF1830-SP) and Ki67 (Thermo Scientific RM 9106-S1) were purchased. TUNEL staining was performed using the TUNEL Assay Kit (Abcam ab206386) according to manufacturer's instructions. Slides were scanned using Panoramic 250 Flash III (3DHISTECH Ltd) and images were captured through Panoramic Viewer software (3DHISTECH Ltd). Human prostate hyperplasia and cancer tissue array samples were purchased from US Biomax (PR753a).

### CytoTOF

Tumor cells were isolated using Mouse Tumor Dissociation Kit (Miltenyi Biotec 130-096-730) and were depleted of red blood cells using RBC Lysis Buffer (BioLegend 420301). Cells were Fc-blocked by CD16/CD32 antibody (clone 2.4G2, BD Biosciences BDB553142) and incubated with CyTOF surface antibody cocktails for 30 minutes at 4°C. Cells were washed with PBS and incubated with Cell-ID Cisplatin (Fluidigm 201064) for dead cell staining. For intracellular staining, cells were permeabilized using Foxp3 Fixation/Permeabilization buffer (eBioscience eBio 00-5523) for 1 hour at room temperature, protected from light. Cells were washed twice and incubated with CyTOF intracellular antibody mix for 1 hour at room temperature, protected from light. For singlet discrimination, cells were washed and incubated with Cell-ID Intercalator-Ir (Fluidigm 201192A) overnight at 4°C. The samples were submitted to the Flow Cytometry and Cellular Imaging Core Facility at MD Anderson Cancer Center, and run using CyTOF instrumentation (DVS Science). CyTOF data were analyzed by FlowJo and Cytobank.

### Primary murine prostate cancer cell culture

Prostate tumors were dissected from *Pten<sup>pc-/-</sup>Smad4<sup>pc-/-</sup>Trp53<sup>c-/-</sup>mTmG* mice and washed in PBS. Tumors were then minced with a blade and dissociated to single cells following the MACS dissociation kit protocol (Miltenyi Biotec 130-096-730). Primary growth medium consisted of DMEM (Life Tech 11995073) with 10% FBS (Life Tech 10082147) and 1× Penicillin-Streptomycin (Life Tech 15140163). GFP-positive cells were sorted and incubated at 37°C in 5% CO<sub>2</sub>. The resulting primary murine prostate cancer cell line was named DX1.

### Inducible Knockdown

Inducible *Chd1* knockdown was constructed by cloning two shRNA targeting murine *Chd1* gene into a doxycycline-inducible plasmid. Sequence of *shChd1* #1: 5'-CCGGTCCGAGCACACATCATAAACTCGAGTTTATGATGTGTGTGCTCGGATTTT TG-3'; Sequence of *shChd1* #2: 5'-CCGGGCCAGGAGACATACAGTATTTCTCGA

GAAATACTGTATGTCTCCTGGCTTTTTG-3'. Lentivirus was packaged in 293T cells and was used to infect DX1. Transduced cells were selected by puromycin (2 ug/mL) and inducible knockdown efficiency was validated by western blot.

### Western Blot Analysis

Cells were lysed on ice using RIPA buffer supplemented with protease and phosphatase inhibitors. Proteins were blotted following standard protocol. Antibodies specific for CHD1 (Cell Signaling, #4351S) and  $\beta$ -actin (Sigma, #A3854) were purchased from the indicated companies.

### MDSC and T Cell Migration Assay

MDSC cells were isolated from murine prostate tumors following the manufacturer's protocols for Mouse Tumor Dissociation Kit (Miltenyi Biotec 130-096-730) and MDSC Isolation Kit (Miltenyi Biotec 130-094-538). Cells ( $10^5$ ) were seeded into the top chamber of a transwell with 200  $\mu$ L FBS-free DMEM with PS; 600 $\mu$ L of conditioned medium was placed into the bottom well. Cells were incubated for 6 hours at 37°C for migration. Three wells were used for each condition. Conditioned medium was collected from the 90-mm plates of indicated cancer cells after 48 hours cultured in FBS-free DMEM, followed by centrifuge to remove the suspending cells. T cells were isolated from murine splenocytes following the manufacturer's protocol for mouse CD8a<sup>+</sup> T Cell Isolation Kit (Miltenyi Biotec #130-104-075). CD8<sup>+</sup> T cells ( $5 \times 10^5$ /well) were used for migration assay as described above.

### MDSC and T Cell Activity Assay

Isolated MDSCs were cultured in the indicated conditioned medium for 24h, followed by FACS analysis using MDSC markers PerCP/Cy5.5-CD11b (BioLegend #101228), APC-Ly6G (BioLegend # 127613), Arg1 (Cell Signaling #93668S) and iNOS (Cell Signaling #13120S). The purified  $5 \times 10^5$  CD8<sup>+</sup> T cells were mixed with pre-washed Dynabeads Mouse T-Activator CD3/CD28 (Life Tech #11456D), and cultured in the indicated conditioned medium for 24h, followed by FACS analysis using CD8<sup>+</sup> T cell markers PerCP/Cy5.5-CD8a (BioLegend #100733), FITC-IFN- $\gamma$  (BD Biosci # 554411) and PE-Ki67 (BioLegend #151209).

### Quantitative RT-PCR and ELISA

RNA was extracted by RNeasy Kit (Qiagen #74034) and reverse transcribed into cDNA using the Superscript III cDNA Synthesis Kit (Life Tech #18080300). Quantitative PCR was performed using the SYBR-Green PCR Kit (Life Tech #4312704) and mouse *IL-6* primers: forward-5'-TAGTCCTTCCTACCCCAATTTCC-3', reverse-5'-TTGGTCCTTAGCCACTCCTTC-3'. To determine IL6 cytokine production by prostate cancer cells, primary cell lines from *Pten*<sup>pc-/-</sup> vs. *PtenChd1*<sup>pc-/-</sup> prostate tumors were cultured for 3 days and the supernatant media were collected. ELISA was performed following the standard protocol of Mouse IL-6 Quantikine ELISA Kit (R&D M6000B).

### RNA-seq and GSEA analysis

Cells were lysed in TRIzol Reagent (Invitrogen; #15596-026), followed by RNeasy Kit (Qiagen #74034) purification using the standard protocol. RNA-seq was conducted by the Sequencing and Microarray Facility (SMF) at MD Anderson Cancer Center. Libraries were made using Illumina's TruSeq kit and sequenced by Illumina HiSeq2000 Sequencer. Raw data were mapped to the hg19 genome, and were then assembled by Cufflinks. The transcriptome of each gene was further quantified. Gene set enrichment analysis (GSEA) was performed to analyze differentially expressed genes.

### ChIP-seq and ChIP-PCR

ChIP was conducted as described using CHD1 antibody (17). Briefly, chromatin from formaldehyde-fixed cells were cross-linked using 1% paraformaldehyde for 10 min and reactions were quenched by addition of 0.125 M glycine for 5 min at room temperature. Cells were lysed with ChIP lysis buffer (10 mM Tris-HCl [pH 8.0], 1 mM EDTA [pH 8.0], 140 mM NaCl, 1% Triton X-100, 0.2% SDS, 0.1% deoxycholic acid) for 30 min on ice. Chromatin fragmentation was performed using a Diagenode BioruptorPico sonicator (30 s on, 30 s off for 45 cycles) to achieve a DNA shear length of 200-500 bp. Solubilized chromatin was then incubated overnight with the appropriate antibody-Dynabead (Life Tech) mixture (anti-CHD1 antibody: Bethyl, #A301-218A; Cell Signaling, #4351S). Immune complexes were then washed three times with RIPA, RIPA-500, and LiCl wash buffers. Elution and reverse-crosslinking were performed in direct elution buffer (10 mM Tris-Cl [pH 8.0], 5 mM EDTA, 300 mM NaCl, 0.5% SDS) with proteinase K (20 mg/ml) at 65°C overnight. Eluted DNA was purified using AMPure beads (Beckman-Coulter). Libraries were prepared using NEBNext Ultra DNA Library kit (E7370). Sequencing was performed using an Illumina HiSeq 2500 instrument. Reads were aligned to hg19 reference genome using BWA (Burrows-Wheeler Aligner). Peak calling and motif calling were performed using Snakemake, a Python 3 based pipeline building tool. For ChIP-PCR analysis, immunoprecipitated chromatin was eluted in 50ul elution buffer. Input and IgG, Chd1, NFkB-immunoprecipitated samples were analyzed by RT-PCRs using IL-6 promoter primers. qRT-PCR was performed with SYBR Green Master Mix. The enrichment of IL-6 promoter sequences in ChIP samples was calculated relative to the IgG negative control.

### ATAC-seq

ATAC-seq was conducted by Active Motif Inc. as described previously (57). In brief, 50,000 cells in duplicates were used for transposition reaction. Twenty-five cycles were used for library amplification. The PCR reactions were performed using the obtained Ct-value. AMPure XP beads were then added to remove fragments bigger than 800 bp and smaller than 100 bp. To determine the average size of each library, the eluted samples were run through a DNA screentape. Qubit dsDNA high sensitivity reagents were used to get the concentration of each library. Finally, all samples were pooled and sequenced on a NextSeq 500. To analyze the data, low-quality reads and duplicate reads were removed, and paired-end reads were aligned to hg38 genome and visualized in UCSC genome browser.

### Luciferase Assay

IL-6-promoter driven luciferase was constructed by cloning the IL-6 promoter region (~1kb) into a pGL4 plasmid. To delete the CHD1 binding site in the IL-6 promoter region, Q5 Site-Directed Mutagenesis Kit (NEB #E0554S) was used. Cells ( $5 \times 10^5$ ) were seeded into 6-well plates and transfected with the constructed pGL4 vector and Renilla control plasmid using Lipofectamine LTX reagent (Thermo Fisher #15338100). After 3 days, cells were washed and analyzed using Dual-Luciferase Reporter Assay System (Promega #E1910). Firefly and Renilla luciferase were read by CLARIOstar microplate reader. Normalization to Renilla luciferase was performed in all samples.

### Orthotopic Prostate Cancer Model and Treatment

All animal procedures were approved by the MD Anderson Animal Care and Use Committee (IACUC Protocol number 00001069). Mice were anaesthetized using ketamine and xylazine. An incision was made in the middle abdomen and the bladder was slowly pulled out with the prostate. DX1 cells were gently injected into the prostate through a Hamilton syringe. Ten microliters of cells ( $5 \times 10^5$ ) were injected per mouse. Animals were imaged by MRI in Small Animal Imaging Facility (SAIF) 12 days after surgery to assess successful tumor implantation. Only orthotopic tumors of similar size were used for the following study. Tumor growth was further monitored by MRI at different time points. Dox treatment was started 12 days after implantation. Antibody intraperitoneal injection was started 13 days after the surgery. The following antibodies were used: anti-mouse PD-1 (Clone RMP1-14, BioXCell); rat IgG1 Isotype control (Clone TNP6A7, BioXCell).

### Chimeric Prostate Cancer Model and Treatment

The chimera cohort was developed as described previously (35). Briefly, derived mES cell lines JH58 and JH61 were genotyped as PB-Cre+ PtenL/L p53L/L Smad4L/L mTmGL/+ LSL-LUCL/+ (CPPSML) and confirmed to contain the Y chromosome. Chimera cohorts were produced by blastocyst microinjection of the mES cells into C57BL/6NTac-Tyrtm1Arte (Taconic, 11971) then followed by uterine implantation into pseudo-pregnant CD-1 (Charles River, 022) or Swiss Webster (Taconic, SW-F) female mice. C57BL/6NTac-Tyrtm1Arte female mice that had achieved successful strain-matched mating after superovulation via timed gonadotropin administration were used as donors for 3.5-day blastocysts. Blastocysts were each micromanipulated to insert roughly 12 individual mES cells into its blastocoel. Injected blastocysts were then implanted into the uteri of pseudo-pregnant females. Each pseudo-pregnant female received up to 14 micromanipulated blastocysts. Chimeras were verified with prostate tumor formation by MRI and assigned into preclinical studies through randomization. Pups were excluded from tumor analysis if they had no tumor formation. For immunotherapy, antibody intraperitoneal injection was started after tumor volume reached  $\sim 50 \text{ mm}^3$ . The following antibodies were injected alone or in combination: anti-mouse PD-1 (Clone RMP1-14, BioXCell); anti-mouse CTLA-4 (Clone 9H10, BioXCell); anti-mouse IL-6 (Clone MP5-20F3, BioXCell); rat IgG1 Isotype control (Clone TNP6A7, BioXCell). Treatment was administrated twice a week for 4 weeks through intraperitoneal injections at a dosage of 200  $\mu\text{g}$ /injection/antibody, and tumor volume was

monitored biweekly. The survival of mice was recorded and tumor tissues were collected and fixed in formalin overnight and embedded in paraffin for molecular analysis.

### Statistical Analysis

Kaplan-Meier survival curves were calculated using GraphPad Prism 7 and compared using the log-rank (Mantel-Cox) test. Pairwise comparisons were performed using the unpaired two-tailed Student's t-test, also done in GraphPad Prism 7. For all experiments with error bars, the standard deviation (STDEV) was calculated and plotted in Excel or GraphPad Prism 7. The 499 TCGA prostate cancer samples were supervised clustered using the R package gplots and MDSC signatures adapted as previously described (33), followed by analysis of CHD1 gene mRNA expression. The correlations between CHD1 and CD15/IL-6/p-Stat3 in human prostate cancer tissues were analyzed using TCGA prostate cancer dataset.

### Supplementary Material

Refer to Web version on PubMed Central for supplementary material.

### Acknowledgement

MD Anderson's Sequencing and Microarray Facility (SMF), and Flow Cytometry and Cellular Imaging Core Facility which are supported by an NCI Cancer Center Support Grant (P30 CA16672); and Baylor College of Medicine GEM Core. This work was supported in part by the Prostate Cancer Foundation (PCF) Young Investigator Award 17YOUN18 (D.Z.), NIH Pathway to Independence Award-NCI 1K99CA226360 (D.Z.), CPRIT Recruitment of First-Time Tenure-Track Faculty Award RR190021 (D.Z.), PCF Challenge Award 17CHAL17 (R.A.D. and Y.A.W.), NIH 1R01CA231349-01A1 (Y.A.W.). MDACC Prostate Cancer Moonshot (R.A.D.)

### REFERENCES

1. Taylor BS, Schultz N, Hieronymus H, Gopalan A, Xiao Y, Carver BS, et al. Integrative Genomic Profiling of Human Prostate Cancer. *Cancer Cell* 2010;18(1):11–22. [PubMed: 20579941]
2. Pourmand G, Ziaee AA, Abedi AR, Mehraei A, Alavi HA, Ahmadi A, et al. Role of PTEN gene in progression of prostate cancer. *Urology journal* 2007;4(2):95–100. [PubMed: 17701929]
3. Wang S, Gao J, Lei Q, Rozengurt N, Pritchard C, Jiao J, et al. Prostate-specific deletion of the murine Pten tumor suppressor gene leads to metastatic prostate cancer. *Cancer Cell* 2003;4(3):209–21 doi S1535610803002150 [pii]. [PubMed: 14522255]
4. Robinson D, Van Allen EM, Wu YM, Schultz N, Lonigro RJ, Mosquera JM, et al. Integrative clinical genomics of advanced prostate cancer. *Cell* 2015;161(5):1215–28 doi 10.1016/j.cell.2015.05.001. [PubMed: 26000489]
5. Grasso CS, Wu YM, Robinson DR, Cao X, Dhanasekaran SM, Khan AP, et al. The mutational landscape of lethal castration-resistant prostate cancer. *Nature* 2012;487(7406):239–43 doi 10.1038/nature11125. [PubMed: 22722839]
6. Carver BS, Chapinski C, Wongvipat J, Hieronymus H, Chen Y, Chandralapaty S, et al. Reciprocal feedback regulation of PI3K and androgen receptor signaling in PTEN-deficient prostate cancer. *Cancer Cell* 2011;19(5):575–86 doi 10.1016/j.ccr.2011.04.008. [PubMed: 21575859]
7. Petrylak DP, Tangen CM, Hussain MH, Lara PN Jr., Jones JA, Taplin ME, et al. Docetaxel and estramustine compared with mitoxantrone and prednisone for advanced refractory prostate cancer. *N Engl J Med* 2004;351(15):1513–20 doi 10.1056/NEJMoa041318. [PubMed: 15470214]
8. Mulholland DJ, Tran LM, Li Y, Cai H, Morim A, Wang S, et al. Cell autonomous role of PTEN in regulating castration-resistant prostate cancer growth. *Cancer Cell* 2011;19(6):792–804 doi 10.1016/j.ccr.2011.05.006. [PubMed: 21620777]

9. Chen Z, Trotman LC, Shaffer D, Lin HK, Dotan ZA, Niki M, et al. Crucial role of p53-dependent cellular senescence in suppression of Pten-deficient tumorigenesis. *Nature* 2005;436(7051):725–30 doi 10.1038/nature03918. [PubMed: 16079851]
10. Ding Z, Wu CJ, Chu GC, Xiao Y, Ho D, Zhang J, et al. SMAD4-dependent barrier constrains prostate cancer growth and metastatic progression. *Nature* 2011;470(7333):269–73 doi 10.1038/nature09677. [PubMed: 21289624]
11. Ding Z, Wu CJ, Jaskelioff M, Ivanova E, Kost-Alimova M, Protopopov A, et al. Telomerase reactivation following telomere dysfunction yields murine prostate tumors with bone metastases. *Cell* 2012;148(5):896–907 doi 10.1016/j.cell.2012.01.039. [PubMed: 22341455]
12. Farnung L, Vos SM, Wigge C, Cramer P. Nucleosome-Chd1 structure and implications for chromatin remodelling. *Nature* 2017;550(7677):539–42 doi 10.1038/nature24046. [PubMed: 29019976]
13. Burkhardt L, Fuchs S, Krohn A, Masser S, Mader M, Kluth M, et al. CHD1 Is a 5q21 Tumor Suppressor Required for ERG Rearrangement in Prostate Cancer. *Cancer Res* 2013;73(9):2795–805 doi 10.1158/0008-5472.Can-12-1342. [PubMed: 23492366]
14. Shenoy TR, Boysen G, Wang MY, Xu QZ, Guo W, Koh FM, et al. CHD1 loss sensitizes prostate cancer to DNA damaging therapy by promoting error-prone double-strand break repair. *Ann Oncol* 2017;28(7):1495–507 doi 10.1093/annonc/mdx165. [PubMed: 28383660]
15. Kari V, Mansour WY, Raul SK, Baumgart SJ, Mund A, Grade M, et al. Loss of CHD1 causes DNA repair defects and enhances prostate cancer therapeutic responsiveness. *EMBO Rep* 2018;19(10) doi 10.15252/embr.201846783.
16. Augello MA, Liu DL, Deonarine LD, Robinson BD, Huang D, Stelloo S, et al. CHD1 Loss Alters AR Binding at Lineage-Specific Enhancers and Modulates Distinct Transcriptional Programs to Drive Prostate Tumorigenesis (vol 35, pg 603, 2019). *Cancer Cell* 2019;35(5):817–9 doi 10.1016/j.ccell.2019.04.012. [PubMed: 31085180]
17. Zhao D, Lu X, Wang G, Lan Z, Liao W, Li J, et al. Synthetic essentiality of chromatin remodelling factor CHD1 in PTEN-deficient cancer. *Nature* 2017;542(7642):484–8 doi 10.1038/nature21357. [PubMed: 28166537]
18. Zhao D, DePinho RA. Synthetic essentiality: Targeting tumor suppressor deficiencies in cancer. *Bioessays* 2017;39(8) doi 10.1002/bies.201700076.
19. Jin X, Ding D, Yan Y, Li H, Wang B, Ma L, et al. Phosphorylated RB Promotes Cancer Immunity by Inhibiting NF-kappaB Activation and PD-L1 Expression. *Mol Cell* 2019;73(1):22–35 e6 doi 10.1016/j.molcel.2018.10.034. [PubMed: 30527665]
20. Karin M, Greten FR. NF-kappaB: linking inflammation and immunity to cancer development and progression. *Nat Rev Immunol* 2005;5(10):749–59 doi 10.1038/nri1703. [PubMed: 16175180]
21. Maia MC, Hansen AR. A comprehensive review of immunotherapies in prostate cancer. *Crit Rev Oncol Hematol* 2017;113:292–303 doi 10.1016/j.critrevonc.2017.02.026. [PubMed: 28427519]
22. Beer TM, Kwon ED, Drake CG, Fizazi K, Logothetis C, Gravis G, et al. Randomized, Double-Blind, Phase III Trial of Ipilimumab Versus Placebo in Asymptomatic or Minimally Symptomatic Patients With Metastatic Chemotherapy-Naive Castration-Resistant Prostate Cancer. *J Clin Oncol* 2017;35(1):40–7 doi 10.1200/JCO.2016.69.1584. [PubMed: 28034081]
23. Kwon ED, Drake CG, Scher HI, Fizazi K, Bossi A, van den Eertwegh AJ, et al. Ipilimumab versus placebo after radiotherapy in patients with metastatic castration-resistant prostate cancer that had progressed after docetaxel chemotherapy (CA184–043): a multicentre, randomised, double-blind, phase 3 trial. *Lancet Oncol* 2014;15(7):700–12 doi 10.1016/S1470-2045(14)70189-5. [PubMed: 24831977]
24. Graff JN, Alumkal JJ, Drake CG, Thomas GV, Redmond WL, Farhad M, et al. Early evidence of anti-PD-1 activity in enzalutamide-resistant prostate cancer. *Oncotarget* 2016;7(33):52810–7 doi 10.18632/oncotarget.10547. [PubMed: 27429197]
25. Gubin MM. Checkpoint blockade cancer immunotherapy targets tumour-specific mutant antigens. *Nature* 2014;515:577–81. [PubMed: 25428507]
26. Wang G, Zhao D, Spring DJ, DePinho RA. Genetics and biology of prostate cancer. *Genes Dev* 2018;32(17–18):1105–40 doi 10.1101/gad.315739.118. [PubMed: 30181359]

27. Kumar V, Patel S, Tcyganov E, Gabrilovich DI. The Nature of Myeloid-Derived Suppressor Cells in the Tumor Microenvironment. *Trends Immunol* 2016;37(3):208–20 doi 10.1016/j.it.2016.01.004. [PubMed: 26858199]
28. Gabrilovich DI, Ostrand-Rosenberg S, Bronte V. Coordinated regulation of myeloid cells by tumours. *Nat Rev Immunol* 2012;12(4):253–68 doi 10.1038/nri3175. [PubMed: 22437938]
29. Vuk-Pavlovi S, Bulur PA, Lin Y, Qin R, Szumlanski CL, Zhao X, et al. Immunosuppressive CD14+HLA-DRlow/- monocytes in prostate cancer. *Prostate* 2010;70(4):443–55 doi 10.1002/pros.21078. [PubMed: 19902470]
30. Brusa D, Simone M, Gontero P, Spadi R, Racca P, Micari J, et al. Circulating immunosuppressive cells of prostate cancer patients before and after radical prostatectomy: Profile comparison. *International Journal of Urology* 2013; 20(10): 971–978 doi 10.1111/iju.12086. [PubMed: 23421558]
31. Bronte V, Wang M, Overwijk WW, Surman DR, Pericle F, Rosenberg SA, et al. Apoptotic death of CD8+ T lymphocytes after immunization: induction of a suppressive population of Mac-1+/Gr-1+ cells. *J Immunol* 1998;161(10):5313–20. [PubMed: 9820504]
32. Talmadge JE, Gabrilovich DI. History of myeloid-derived suppressor cells. *Nat Rev Cancer* 2013;13(10):739–52 doi 10.1038/nrc3581. [PubMed: 24060865]
33. Wang G, Lu X, Dey P, Deng P, Wu CC, Jiang S, et al. Targeting YAP-Dependent MDSC Infiltration Impairs Tumor Progression. *Cancer Discov* 2016;6(1):80–95 doi 10.1158/2159-8290.CD-15-0224. [PubMed: 26701088]
34. Moreira D, Adamus T, Zhao X, Su YL, Zhang Z, White SV, et al. STAT3 Inhibition Combined with CpG Immunostimulation Activates Antitumor Immunity to Eradicate Genetically Distinct Castration-Resistant Prostate Cancers. *Clin Cancer Res* 2018;24(23):5948–62 doi 10.1158/1078-0432.CCR-18-1277. [PubMed: 30337279]
35. Lu X, Horner JW, Paul E, Shang X, Troncoso P, Deng P, et al. Effective combinatorial immunotherapy for castration-resistant prostate cancer. *Nature* 2017;543(7647):728–32 doi 10.1038/nature21676. [PubMed: 28321130]
36. Augello MA, Liu D, Deonarine LD, Robinson BD, Huang D, Stelloo S, et al. CHD1 Loss Alters AR Binding at Lineage-Specific Enhancers and Modulates Distinct Transcriptional Programs to Drive Prostate Tumorigenesis. *Cancer Cell* 2019;35(5):817–9 doi 10.1016/j.ccell.2019.04.012. [PubMed: 31085180]
37. Bendall SC, Simonds EF, Qiu P, Amir el AD, Krutzik PO, Finck R, et al. Single-cell mass cytometry of differential immune and drug responses across a human hematopoietic continuum. *Science* 2011;332(6030):687–96 doi 10.1126/science.1198704. [PubMed: 21551058]
38. Bandura DR, Baranov VI, Ornatsky OI, Antonov A, Kinach R, Lou X, et al. Mass cytometry: technique for real time single cell multitarget immunoassay based on inductively coupled plasma time-of-flight mass spectrometry. *Anal Chem* 2009;81(16):6813–22 doi 10.1021/ac901049w. [PubMed: 19601617]
39. Amir el AD, Davis KL, Tadmor MD, Simonds EF, Levine JH, Bendall SC, et al. viSNE enables visualization of high dimensional single-cell data and reveals phenotypic heterogeneity of leukemia. *Nat Biotechnol* 2013;31(6):545–52 doi 10.1038/nbt.2594. [PubMed: 23685480]
40. Yu H, Pardoll D, Jove R. STATs in cancer inflammation and immunity: a leading role for STAT3. *Nat Rev Cancer* 2009;9(11):798–809 doi 10.1038/nrc2734. [PubMed: 19851315]
41. Hodge DR, Hurt EM, Farrar WL. The role of IL-6 and STAT3 in inflammation and cancer. *Eur J Cancer* 2005;41(16):2502–12 doi 10.1016/j.ejca.2005.08.016. [PubMed: 16199153]
42. Wu CT, Hsieh CC, Lin CC, Chen WC, Hong JH, Chen MF. Significance of IL-6 in the transition of hormone-resistant prostate cancer and the induction of myeloid-derived suppressor cells. *J Mol Med (Berl)* 2012;90(11):1343–55 doi 10.1007/s00109-012-0916-x. [PubMed: 22660275]
43. Chen MF, Kuan FC, Yen TC, Lu MS, Lin PY, Chung YH, et al. IL-6-stimulated CD11b+ CD14+ HLA-DR- myeloid-derived suppressor cells, are associated with progression and poor prognosis in squamous cell carcinoma of the esophagus. *Oncotarget* 2014;5(18):8716–28 doi 10.18632/oncotarget.2368. [PubMed: 25238263]



44. Sumida K, Wakita D, Narita Y, Masuko K, Terada S, Watanabe K, et al. Anti-IL-6 receptor mAb eliminates myeloid-derived suppressor cells and inhibits tumor growth by enhancing T-cell responses. *Eur J Immunol* 2012;42(8):2060–72 doi 10.1002/eji.201142335. [PubMed: 22653638]
45. Abad C, Nobuta H, Li J, Kasai A, Yong WH, Waschek JA. Targeted STAT3 disruption in myeloid cells alters immunosuppressor cell abundance in a murine model of spontaneous medulloblastoma. *J Leukoc Biol* 2014;95(2):357–67 doi 10.1189/jlb.1012531. [PubMed: 24068730]
46. Highfill SL, Cui Y, Giles AJ, Smith JP, Zhang H, Morse E, et al. Disruption of CXCR2-mediated MDSC tumor trafficking enhances anti-PD1 efficacy. *Sci Transl Med* 2014;6(237):237ra67 doi 10.1126/scitranslmed.3007974.
47. Liao W, Overman MJ, Boutin AT, Shang X, Zhao D, Dey P, et al. KRAS-IRF2 Axis Drives Immune Suppression and Immune Therapy Resistance in Colorectal Cancer. *Cancer Cell* 2019;35(4):559–72 e7 doi 10.1016/j.ccell.2019.02.008. [PubMed: 30905761]
48. Libermann TA, Baltimore D. Activation of interleukin-6 gene expression through the NF-kappa B transcription factor. *Mol Cell Biol* 1990;10(5):2327–34 doi 10.1128/mcb.10.5.2327. [PubMed: 2183031]
49. Chen P, Cescon M, Bonaldo P. Collagen VI in cancer and its biological mechanisms. *Trends Mol Med* 2013;19(7):410–7 doi 10.1016/j.molmed.2013.04.001. [PubMed: 23639582]
50. Burkhardt L, Fuchs S, Krohn A, Masser S, Mader M, Kluth M, et al. CHD1 is a 5q21 tumor suppressor required for ERG rearrangement in prostate cancer. *Cancer research* 2013;73(9):2795–805 doi 10.1158/0008-5472.CAN-12-1342. [PubMed: 23492366]
51. Kantoff PW, Higano CS, Shore ND, Berger ER, Small EJ, Penson DF, et al. Sipuleucel-T immunotherapy for castration-resistant prostate cancer. *N Engl J Med* 2010;363(5):411–22 doi 10.1056/NEJMoa1001294. [PubMed: 20818862]
52. Jiang H, Hegde S, Knolhoff BL, Zhu Y, Herndon JM, Meyer MA, et al. Targeting focal adhesion kinase renders pancreatic cancers responsive to checkpoint immunotherapy. *Nat Med* 2016;22(8):851–60 doi 10.1038/nm.4123. [PubMed: 27376576]
53. De Henau O, Rausch M, Winkler D, Campesato LF, Liu C, Cymerman DH, et al. Overcoming resistance to checkpoint blockade therapy by targeting PI3Kgamma in myeloid cells. *Nature* 2016;539(7629):443–7 doi 10.1038/nature20554. [PubMed: 27828943]
54. Johnson DE, O’Keefe RA, Grandis JR. Targeting the IL-6/JAK/STAT3 signalling axis in cancer. *Nat Rev Clin Oncol* 2018;15(4):234–48 doi 10.1038/nrclinonc.2018.8. [PubMed: 29405201]
55. Wallner L, Dai J, Escara-Wilke J, Zhang J, Yao Z, Lu Y, et al. Inhibition of interleukin-6 with CNTO328, an anti-interleukin-6 monoclonal antibody, inhibits conversion of androgen-dependent prostate cancer to an androgen-independent phenotype in orchiectomized mice. *Cancer Res* 2006;66(6):3087–95 doi 10.1158/0008-5472.CAN-05-3447. [PubMed: 16540658]
56. Dorff TB, Goldman B, Pinski JK, Mack PC, Lara PN Jr., Van Veldhuizen PJ Jr., et al. Clinical and correlative results of SWOG S0354: a phase II trial of CNTO328 (siltuximab), a monoclonal antibody against interleukin-6, in chemotherapy-pretreated patients with castration-resistant prostate cancer. *Clin Cancer Res* 2010;16(11):3028–34 doi 10.1158/1078-0432.CCR-09-3122. [PubMed: 20484019]
57. Buenrostro JD, Giresi PG, Zaba LC, Chang HY, Greenleaf WJ. Transposition of native chromatin for fast and sensitive epigenomic profiling of open chromatin, DNA-binding proteins and nucleosome position. *Nat Methods* 2013;10(12):1213–8 doi 10.1038/nmeth.2688. [PubMed: 24097267]

**STATEMENT OF SIGNIFICANCE**

We demonstrate a critical role of CHD1 in MDSC recruitment and discover CHD1/IL-6 as a major regulator of the immunosuppressive TME of PTEN-deficient prostate cancer. Pharmacologic inhibition of IL-6 in combination with immune checkpoint blockade elicits robust anti-tumor responses in prostate cancer.

Author Manuscript

Author Manuscript

Author Manuscript

Author Manuscript

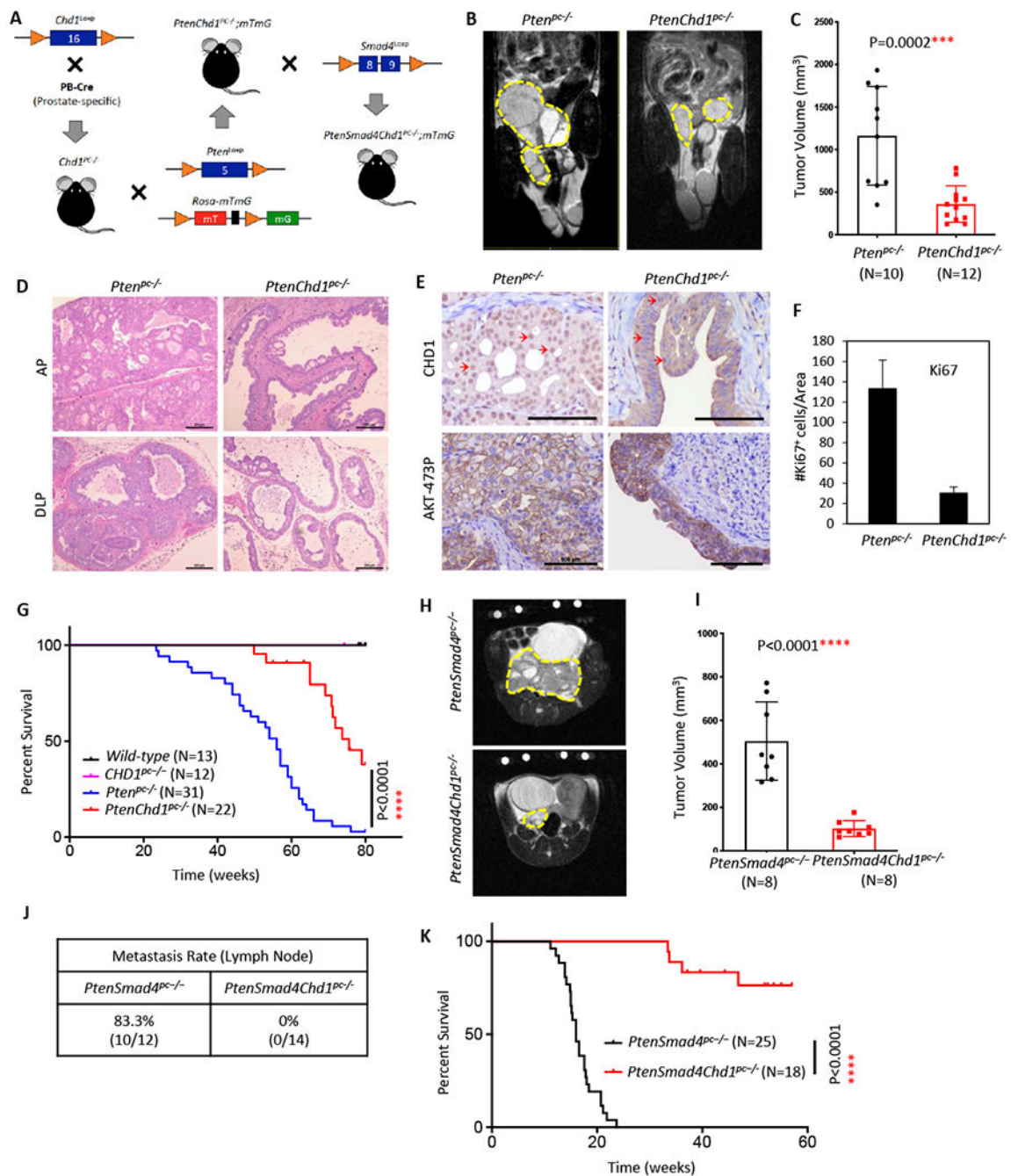


**Figure 1. Genetic deletion of *Chd1* inhibits development of PTEN-null prostate cancer** (A) GEM model design: Conditional knockout alleles of *Chd1*<sup>Loxp</sup>, *Pten*<sup>Loxp</sup>, and *Smad4*<sup>Loxp</sup> were crossed with prostate-specific *PB-Cre* and *Rosa-mTmG* to establish a prostate-specific *PtenChd1* or *PtenSmad4Chd1* knockout prostate cancer mouse model. *Pten*<sup>pc/-</sup>, *PB-Cre Pten*<sup>L/L</sup>; *Chd1*<sup>pc/-</sup>, *PB-Cre Chd1*<sup>L/L</sup>; *PtenChd1*<sup>pc/-</sup>, *PB-Cre Pten*<sup>L/L</sup> *Chd1*<sup>L/L</sup>; *PtenSmad4*<sup>pc/-</sup>, *PB-Cre Pten*<sup>L/L</sup> *Smad4*<sup>L/L</sup>; *PtenSmad4*<sup>pc/-</sup>, *PB-Cre Pten*<sup>L/L</sup> *Smad4*<sup>L/L</sup>; *PtenSmad4Chd1*<sup>pc/-</sup>, *PB-Cre Pten*<sup>L/L</sup> *Smad4*<sup>L/L</sup> *Chd1*<sup>L/L</sup>. (B-C) Prostate tumor MRI and tumor volume of *Pten*<sup>pc/-</sup> and *PtenChd1*<sup>pc/-</sup> mice at 12 months of age. (D) H&E

staining of prostate tumors from 7-month old *Pten<sup>pc-/-</sup>* and *PtenChd1<sup>pc-/-</sup>* mice. AP: anterior prostate; DLP: dorsal-lateral prostate. Scale bar: 200  $\mu\text{m}$ . (E) IHC staining of CHD1 and phospho-AKT (Ser473) markers and (F) quantification of Ki67<sup>+</sup> cells of *Pten<sup>pc-/-</sup>* vs. *PtenChd1<sup>pc-/-</sup>* prostate tumors. Scale bar: 100  $\mu\text{m}$ . (G) Kaplan-Meier survival curve of wild type, *Chd1<sup>pc-/-</sup>*, *Pten<sup>pc-/-</sup>* and *PtenChd1<sup>pc-/-</sup>* mice. (H-I) MRI and tumor volume of prostate tumors from *PtenSmad4<sup>pc-/-</sup>* mice with or without *Chd1* deletion at 4 months of age. (J) Lymph node metastasis rate and (K) Kaplan-Meier survival curve of *PtenSmad4<sup>pc-/-</sup>* and *PtenSmad4Chd1<sup>pc-/-</sup>* mice.

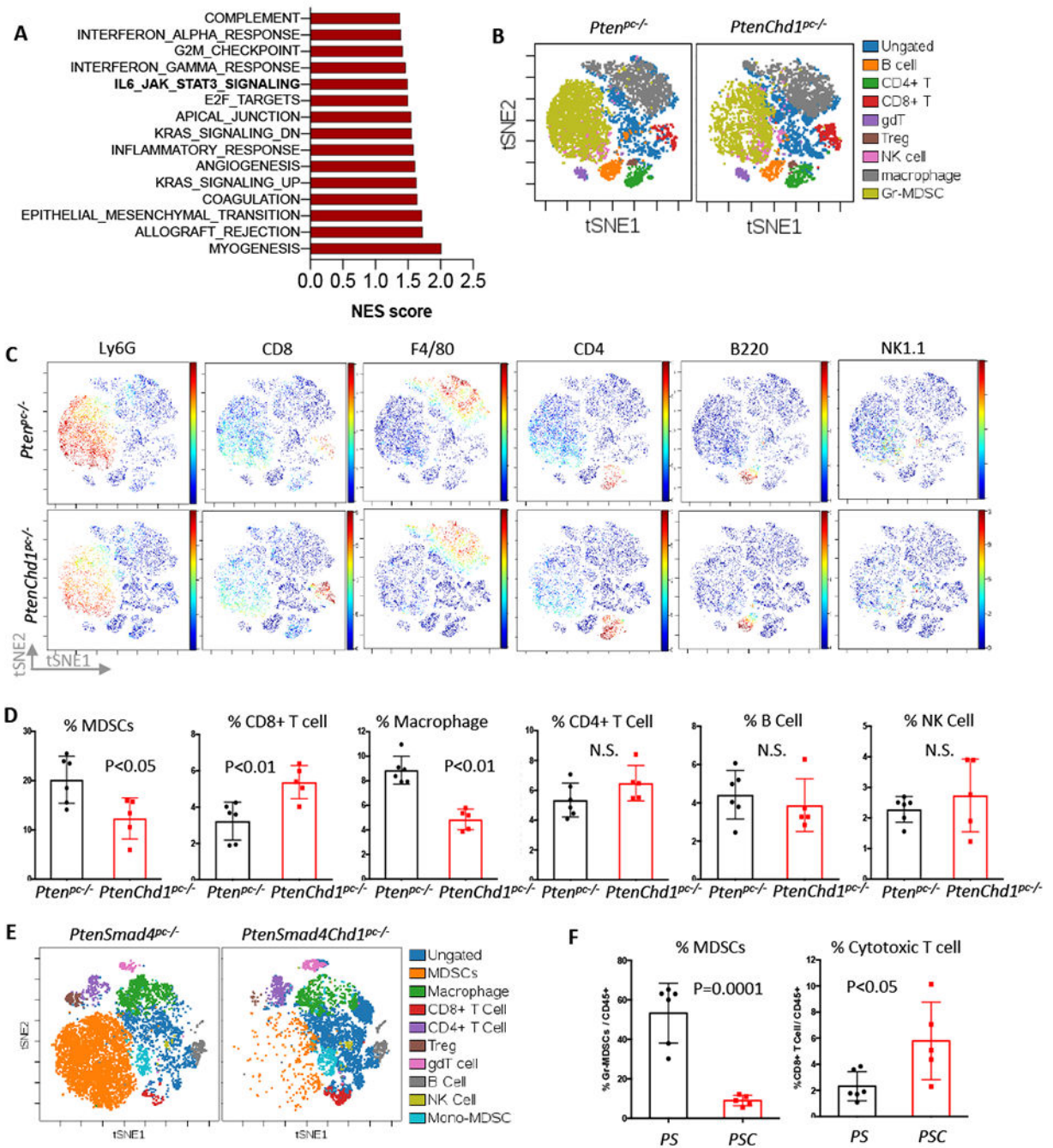


**Figure 2. CHD1 promotes an immunosuppressive TME in prostate cancer**

(A) Top 15 down-regulated pathways in *PtenChd1<sup>pc/-</sup>* prostate tumors. Pathways highlighted in red are immune response related pathways. NES: normalized enrichment score. (B-D) Immunoprofiling of *Pten<sup>pc/-</sup>* vs. *PtenChd1<sup>pc/-</sup>* prostate tumors using CyTOF. (B,C) viSNE plots colored by relative expression of CyTOF markers, with populations indicated, and (D) quantification of each tumor infiltrating immune cell population. (E,F) Immunoprofiling of *PtenSmad4<sup>pc/-</sup>* vs. *PtenSmad4Chd1<sup>pc/-</sup>* prostate tumors using CyTOF.

(E) viSNE plots and (F) quantification of tumor infiltrating immune cell populations. PS, *PtenSmad4<sup>pc-/-</sup>*; PSC, *PtenSmad4Chd1<sup>pc-/-</sup>*

Author Manuscript

Author Manuscript

Author Manuscript

Author Manuscript

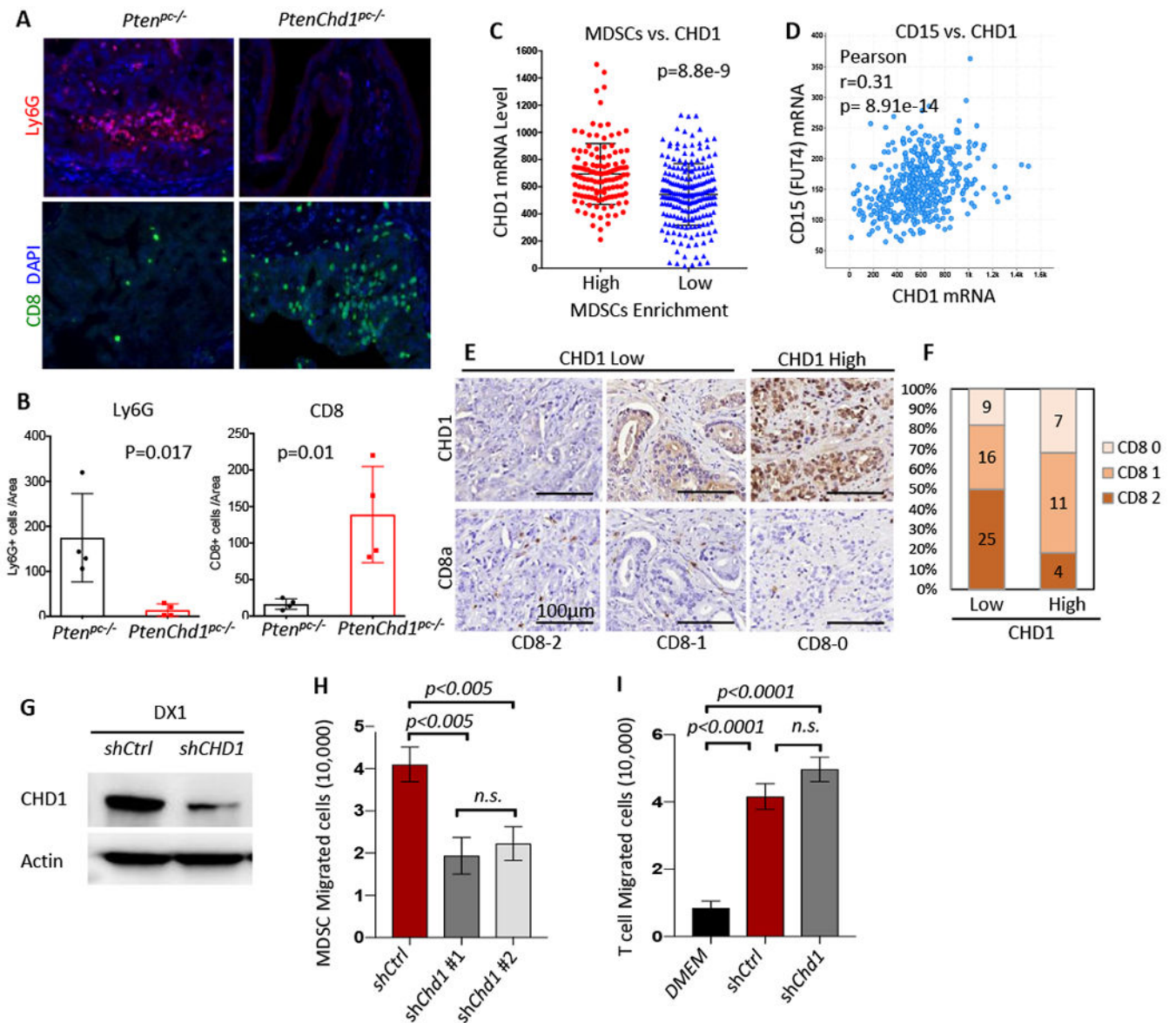


**Figure 3. CHD1 controls MDSC recruitment**

(A,B) Immunofluorescence staining and quantification of MDSC marker (Ly6G) and CD8<sup>+</sup> T cell marker (CD8a) in *Pten<sup>pc-/-</sup>* vs. *PtenChd1<sup>pc-/-</sup>* prostate tumors. (C) CHD1 expression correlates with MDSC enrichment in human prostate tumors. (D) Correlation analysis of CHD1 and MDSC marker CD15 expression in TCGA dataset. (E,F) Correlation analysis of CD8<sup>+</sup> T cells infiltration and CHD1 expression in human prostate cancer samples (n = 72; r = -0.273; p = 0.02). CHD1 expression: Low or High. CD8 score: 0-2. Scale bar: 100  $\mu$ m. (G) Western blot of CHD1-depleted or control murine prostate cancer cells. (H,I) *In vitro* migration assay of MDSCs and T cells in the conditioned medium collected from CHD1-depleted or control murine prostate cancer cells.

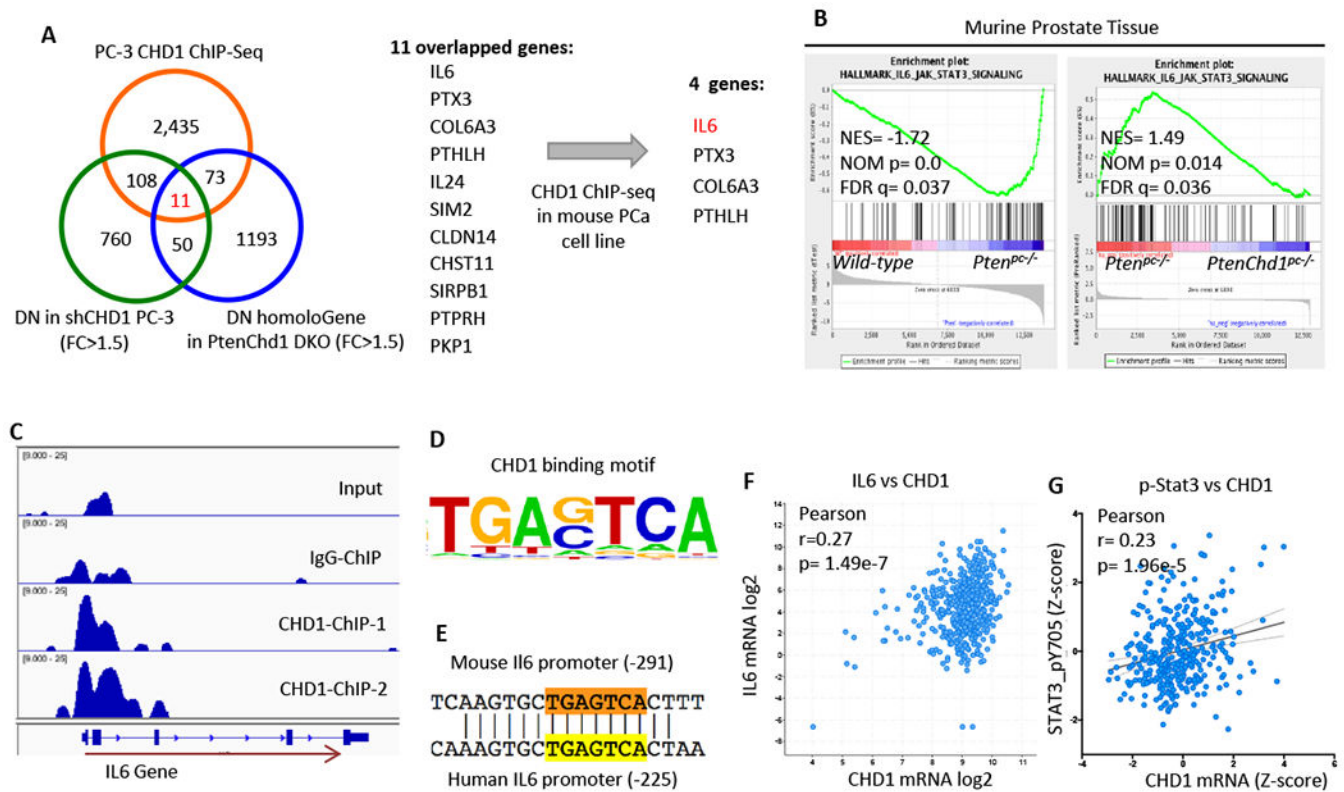


**Figure 4. *IL-6* is a direct target gene of CHD1**

(A) Venn diagram of CHD1 directly regulated genes identified by ChIP-seq and differential expression genes in CHD1 depletion PC-3 or murine prostate tumors. The overlapping 11 genes are considered direct target genes of CHD1. (B) GSEA analysis of wild type, *Pten<sup>pc-/-</sup>* vs. *PtenChd1<sup>pc-/-</sup>* prostate samples indicates the IL-6-Stat3 pathway regulated by PTEN-CHD1 axis. (C) ChIP-seq in *Pten* deletion prostate cancer cells revealed binding peaks of CHD1 on IL-6 gene promoter region. CHD1-ChIP-1: CHD1 antibody from CST; CHD1-ChIP-2: CHD1 antibody from Bethyl. (D,E) ChIP-seq analysis of top CHD1 binding motif (TGAG/CCTCA), which is conserved in human and murine IL-6 promoter. (F,G) Correlation analysis of CHD1 expression and IL-6 or phospho-Stat3 level in human prostate tumors (TCGA data)



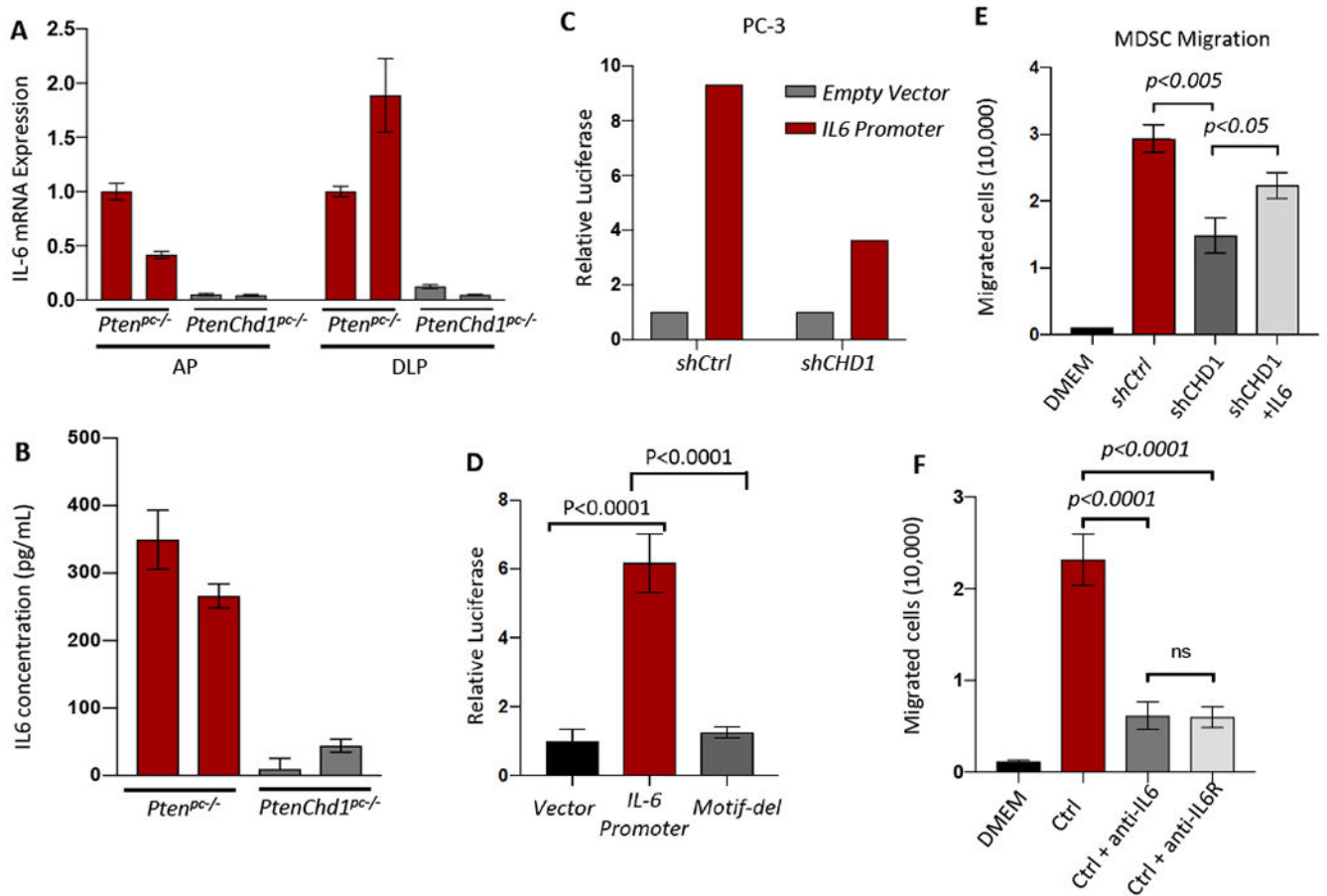


**Figure 5. IL-6 serves as a key mediator for MDSC recruitment induced by CHD1**  
 (A) *IL-6* gene expression of *Pten<sup>pc-/-</sup>* vs. *PtenChd1<sup>pc-/-</sup>* prostate tumors determined using qPCR. (B) ELISA assay of IL-6 in *Pten<sup>pc-/-</sup>* vs. *PtenChd1<sup>pc-/-</sup>* prostate tumors. (C) Luciferase assay reveals CHD1 directly regulates the activation of IL6 promoter. (D) Luciferase assay with wild type or depleted CHD1 binding motif in the *IL6* promoter region. (E,F) *In vitro* MDSC migration assay in the presence of IL6 recombinant proteins in CHD1 depletion conditioned medium (E) or IL-6 or IL-6R inhibitors in wild type conditioned medium (F).

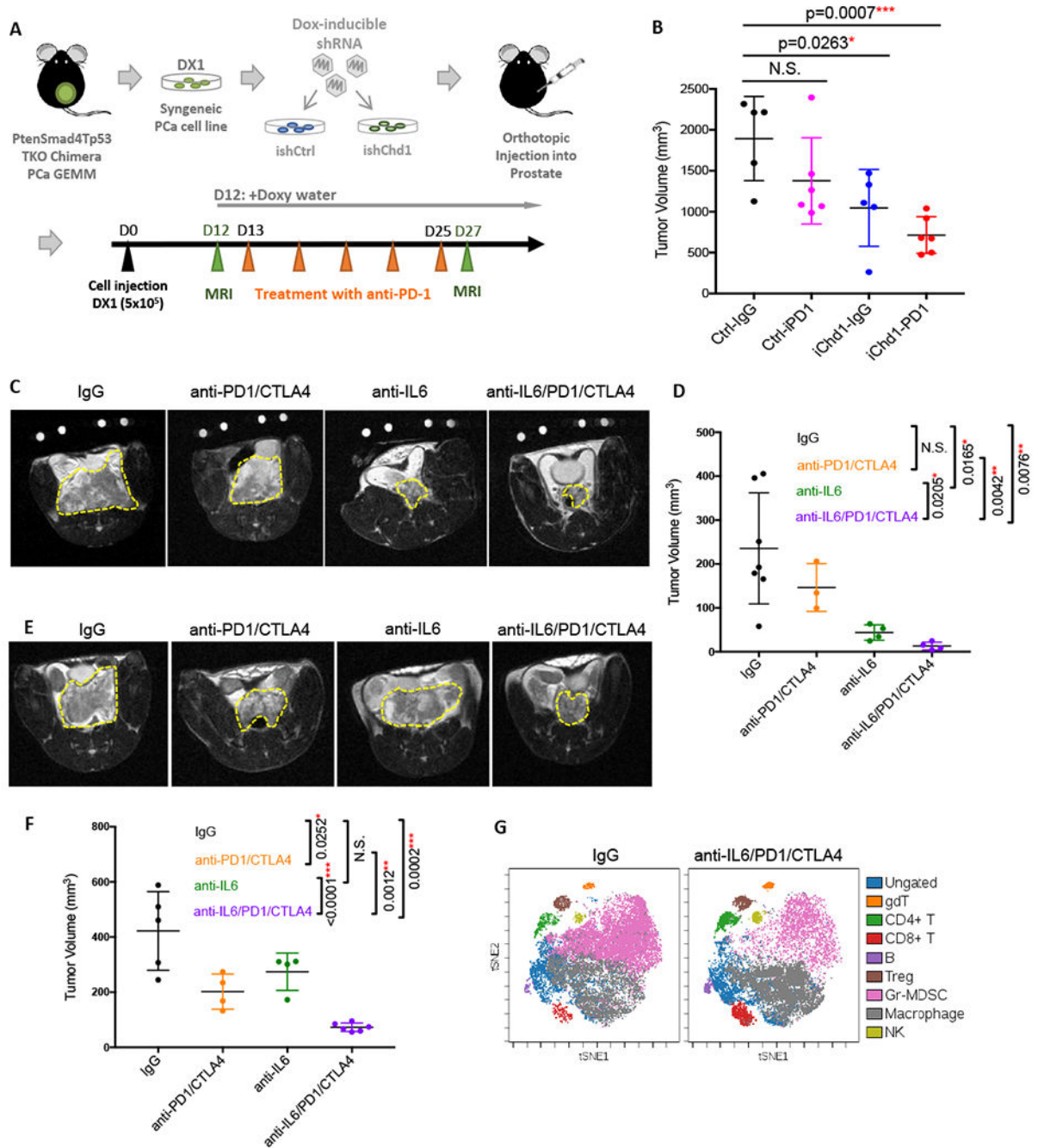


**Figure 6. Synergistic anti-tumor effect of CHD1/IL-6 inhibition in combination with ICI in prostate cancer**

(A) Schematic illustrating the generation of inducible-*shCHD1* DX1 cells and orthotopic prostate cancer mouse model, followed by the treatment with Doxycycline and anti-PD1. (B) Tumor volume was measured by MRI after 2 weeks of treatment. (C-D) The anti-tumor effects of combinatorial IL-6 inhibition and anti-PD1/CTLA4 dual blockade were evaluated in the “CPPSML” chimeric prostate cancer model. Tumor growth was monitored by MRI bi-weekly; MRI images (C) and volumes (D) after 6 treatments are shown here. (E-F) MRI

imaging and tumor volume after single, dual or triple blockades of IL-6/PD1/CTLA-4 in the *PtenSmad4<sup>pc-/-</sup>* prostate cancer GEM model. (G) viSNE plots of tumor infiltrating immune cells in *PtenSmad4<sup>pc-/-</sup>* prostate tumors treated with IgG or triple blockades of IL-6/PD1/CTLA-4.

Author Manuscript

Author Manuscript

Author Manuscript

Author Manuscript

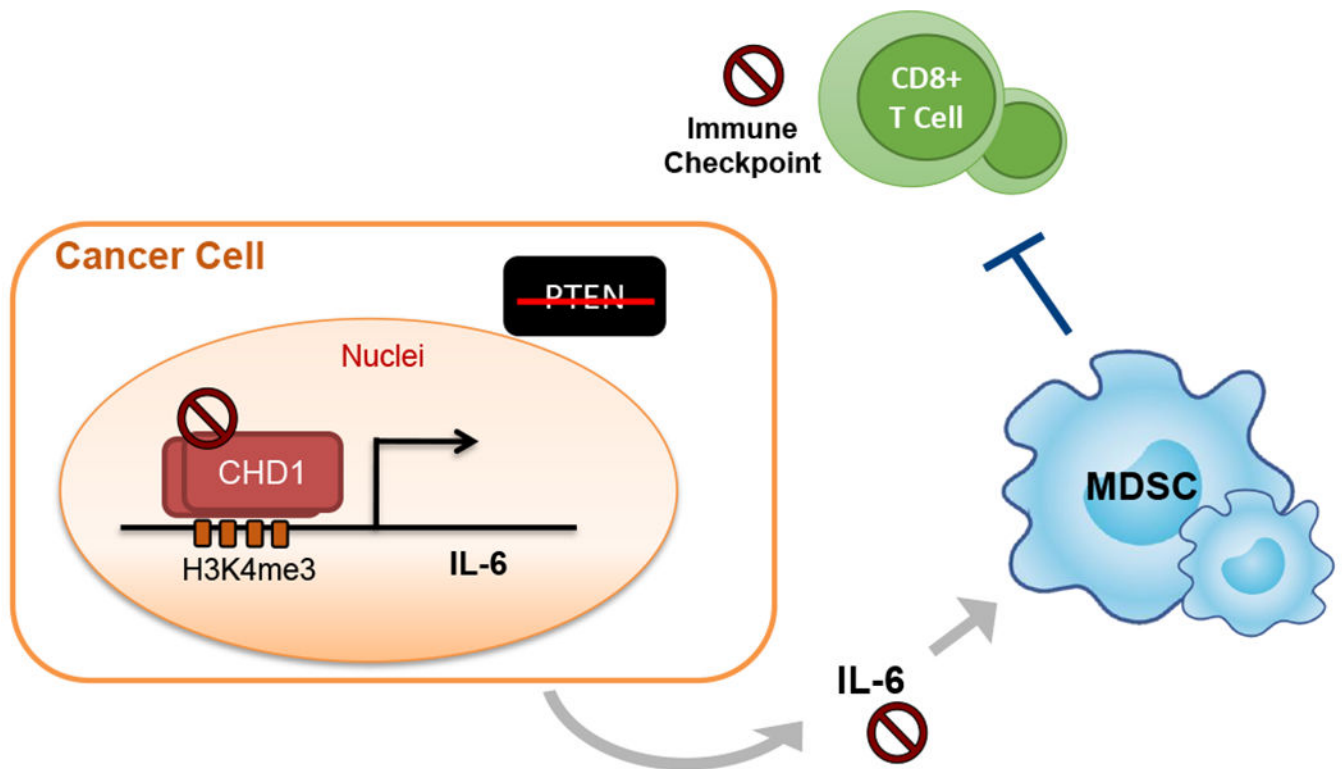


**Figure 7. CHD1 contributes to the remodeling of the TME and resistance to ICI**

In *PTEN*-loss prostate cancer cells, CHD1 is stabilized and interacts with active epigenetic marker trimethylation of histone H3 at lysine 4 (H3K4me3) (17). IL-6 serves as a direct target gene of CHD1 and contributes to recruit immunosuppressive MDSCs, resulting in the inhibition of CD8<sup>+</sup> T cells in prostate tumor. Disruption of the CHD1-IL-6 axis suppresses MDSC infiltration and boosts intratumor CD8<sup>+</sup> T cells. In combination with immune checkpoint inhibition, IL-6 inhibition shows durable therapeutic effects on *PTEN*-deficient prostate cancer.